# Land Surface Temperature with Land Cover Dynamics: Multi-Resolution, Spatio-Temporal Data Analysis of Greater Bangalore, India

**Ramachandra, T. V.,[1] and Uttam Kumar[2]**
[1]Energy and Wetlands Research Group, Centre for Ecological Sciences & Centre for Infrastructure, Sustainable Transportation and Urban Planning [CiSTUP], Indian Institute of Science, Bangalore, India, E-mail: cestvr@ces.iisc.ernet.in, energy@ces.iisc.ernet.in
[2]Centre for Sustainable Technologies, Department of Management Studies, Indian Institute of Science, Bangalore, India

**Abstract**
*Bangalore is experiencing unprecedented urbanisation in recent times due to concentrated developmental activities with impetus on IT (Information Technology) and BT (Biotechnology) sectors. The concentrated developmental activities has resulted in the increase in population and consequent pressure on infrastructure, natural resources, ultimately giving rise to a plethora of serious challenges such as urban flooding, climate change, etc. One of the perceived impact at local levels is the increase in sensible heat flux from the land surface to the atmosphere, which is also referred as heat island effect. In this communication, we report the changes in land surface temperature (LST) with respect to land cover changes during 1973 to 2007. A novel technique combining the information from sub-pixel class proportions with information from classified image (using signatures of the respective classes collected from the ground) has been used to achieve more reliable classification. The analysis showed positive correlation with the increase in paved surfaces and LST. 466% increase in paved surfaces (buildings, roads, etc.) has lead to the increase in LST by about 2 ºC during the last 2 decades, confirming urban heat island phenomenon. LSTs' were relatively lower (~ 4 to 7 ºC) at land uses such as vegetation (parks/forests) and water bodies which act as heat sinks.*

## 1. Introduction

Many cities in developing countries are now undergoing rapid urbanisation evident from the increase in urban population from 13% (220 million) in 1900, to 29% (732 million) in 1950, to 49% (3.2 billion) in 2005 and is projected to rise to 60% (4.9 billion) by 2030 (WUP, 2005). Accurate and timely information in land use (LU) and LU changes is crucial for long-term economic development planning and also for short-term land management. Increase in paved land covers (LC) consequent to the concentrated human activities often leads to increased land surface temperatures (LST). Enhanced LST in certain urban pockets compared to its immediate surroundings consequent to the increase in paved surfaces is known as urban heat island (UHI) phenomenon (Landsbeg, 1981). Specifically, surface and atmospheric temperatures are increased by anthropogenic heat discharge due to energy consumption, increased land surface coverage by artificial materials having high heat capacities and conductivities, and the associated decreases in vegetation and water impervious surfaces, which reduce surface temperature through evapotranspiration (Kato and Yamaguchi, 2005). Temperatures have been monitored through space borne remote sensing (RS) sensors, which measure top of the atmosphere (TOA) radiances in the Thermal Infrared (TIR) region. TOA radiance is the net result of emitted radiance from the Earth's surface, upwelling radiance from the atmosphere, and downwelling radiance from the sky. Brightness temperatures (also known as blackbody temperatures) can be derived from the TOA radiance (Dash et al., 2002). These brightness temperatures are further corrected with spectral emissivity values prior to the computation of LST to account for the roughness properties of the land surface, the amount and nature of vegetation cover, and the thermal properties and moisture content of the soil (Friedl, 2002). However, lack of knowledge of emissivity can introduce an error ranging from 0.2 to 1.2 K for mid-latitude summers and from 0.8 to 1.4 K for the winter conditions for an emissivity of 0.98 and at the ground height of 0 km (Dash et al., 2002). Two approaches have been developed to recover LST from multispectral TIR imagery (Schmugge et al., 1998). The first approach utilises a radiative transfer equation to correct the at-sensor radiance to surface radiance, followed by an emissivity model to separate the surface radiance

into temperature and emissivity (Friedl, 2002). The second approach applies the split-window technique for sea surfaces to land surfaces, assuming that the emissivity in the channels used for the split window is similar (Dash et al., 2002). TIR region corresponding to 8 -14 μm in the electromagnetic spectrum is being used in quantifying the thermal urban environment (as per Wien's displacement law) as well as mapping heat islands in the urban areas. Currently available RS data pertaining to visible, near infrared (NIR) and thermal range in different spatial resolution and temporal coverage are used for LU/LC classification and LST estimations. Spatial resolution of the data plays an important role in classification scheme and studies have been carried out to understand the role of various resolutions for LU classification. Multi-sensor RS data were analysed for terrain cover classification over the Greater Sydney region by Forghani et al., (2007). National terrain surface roughness was generated, using MODIS (Level 1-areas with no major towns), Landsat/ASTER/SPOT 2/4 (Level 2-areas with major towns), SPOT-5 (Level 3-areas with capital/major cities), and IKONOS/QuickBird (Level 4-areas containing significant critical infrastructure). The study highlights that Landsat TM/ETM+ imagery is suited for derivation of 30 m and 100 m resolution terrain maps. UHI was investigated earlier through LST measurements using NOAA AVHRR data (Li et al., 2004, Balling and Brazell, 1988, Gallo et al., 1993, Gallo and Owen, 1998 and Kidder and Wu, 1987), TM TIR data (Carnahan and Larson, 1990), Landsat TM data (Tanaka et al., 2005), ASTER and ETM+ data (Kato and Yamaguchi, 2005), Landsat-5 TM and Landsat-7 ETM+ data (Nikolakopoulos et al., 2003, Stathopoulou and Cartalis, 2007 and Weng et al., 2004), Corine LC with Landsat ETM+ data (Stathopoulou and Cartalis, 2007). However, there are no studies to understand the LST with LU dynamics in a rapidly urbanising region such as Greater Bangalore. Hence, the objective of this study is to investigate the LST with LU dynamics to understand the urban heat island phenomenon in Greater Bangalore considering multi - senor, multi - resolution and temporal RS data acquired through space borne sensors. This involved:

i) Temporal LU change analysis (during 1973 to 2007);
ii) Computation of LST and NDVI (Normalized Difference Vegetation Index) from Landsat TM (1992) and MODIS data (2000 and 2007) of summer month;
iii) Investigation of the role of NDVI in LST;
iv) Deriving sub-pixel proportion of LU using linear mixture model (LMM) on bands of ETM+ (excluding thermal and panchromatic) and investigate its relationship with LST;
v) Deriving improved supervised classified LC map through Bayesian classifier using abundance values obtained from LMM as a prior probability along with information from classified map obtained using spectral signatures (training polygons).

## 2. Data and Methods

*2.1Data*

Data used in the study are Landsat MSS (1973), TM (1992), IRS LISS-III MSS (1999), Landsat ETM+ (2000), IRS LISS-III (2006), MODIS 7 bands reflectance product (2002, 2007), MODIS Land Surface Temperature/Emissivity (V004 and V005): 8-Day, L3 Global 1km products (2000, 2007) and Google Earth (http://earth.google.com).

*2.2 Study Area*

Greater Bangalore is the principal administrative, cultural, commercial, industrial, and knowledge capital of the state of Karnataka with an area of 741 $km^2$ and lies between the latitudes 12°39′00″ to 13°13′00″ N and longitude 77°22′00″ to 77°52′00″ E. Bangalore city administrative jurisdiction was widened in 2006 by merging the existing area of Bangalore city spatial limits with 8 neighboring Urban Local Bodies (ULBs) and 111 Villages of Bangalore Urban District. Thus, Bangalore has grown spatially more than ten times since 1949 (69 $km^2$). Now, Bangalore (Figure 1) is the fifth largest metropolis in India currently with a population of about 7 million (Ramachandra and Kumar, 2008).

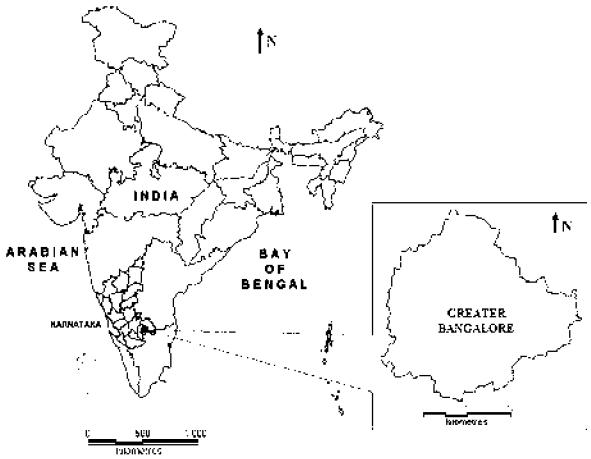


Figure 1: Study area – Greater Bangalore, India

*2.3 Methods*

*2.3.1 Land use analysis*

This was done with Landsat data of 1973 (79 m spatial resolution), 1992 and 2000 (30 m), IRS

LISS-III data of 1999 and 2006 (23.5 m) and MODIS data of 2002 and 2007 (250 m to 500 m spatial resolution) using supervised pattern classifiers based on Gaussian maximum likelihood (GML) estimation followed by a Bayesian statistical approach. This technique quantifies the tradeoffs between various classification decisions using probability and costs that accompany such decisions (Duda et al., 2000). It makes assumptions that the decision problem is posed in probabilistic terms, and that all of the relevant probability values are known with a number of design samples or training data collected from field that are particular representatives of the patterns to be classified. The mean and covariance are computed using maximum likelihood estimation with the best estimates that maximises the probability of the pixels falling into one of the classes. LU analysis considering temporal data (1973, 1992, 1999, 2000, 2002, 2006 and 2007) was done using the open source programs (i.gensig, i.class and i.maxlik) of Geographic Resources Analysis Support System (http://wgbis.ces.iisc.ernet.in/grass).

*2.3.2 Change detection*

LU change detection is performed by change/no-change recognition followed by boundary delineation on images of two different time periods. Pixels which show significant changes are checked and validated on the ground and the boundaries of the changed patches are category wise delineated. This is supplemented with visual interpretation and online digitisation. Many LU change detection techniques have been developed, but no single algorithm is suitable for all cases (Lu et al., 2004), as the implementation of change detection analysis is dependent on the data itself (Zhang and Zhang, 2007). Bi-temporal multispectral images have been analysed to understand LU dynamics through:

- ***Principal Component Analysis*** (PCA) – PCA has been an effective tool for change detection (Fung and LeDrew, 1987 and Michener and Houhoulis, 1997). Major components of the time two ($t_2$) data are subtracted from the corresponding components of the time one ($t_1$) data to obtain differences related to changes in LU. This method provides a better result than simple image differencing when the radiometric differences between the two images are too large due to different imaging circumstances and cannot be effectively dealt with by the radiometric normalisation process (Zhang and Zhang, 2007). Landsat MSS (1973) and IRS LISS-III (2006) scenes having different radiometry were used with PCA to understand the overall changes across a period of 33 years.
- ***Tasseled Cap*** (TC) or Kauth-Thomas (KT) transformation – Here, multi-temporal TM and ETM+ data are transformed into the brightness-greenness-wetness space, then changed areas are generated by differencing the brightness (ΔB) and greenness (ΔG) values (Kauth and Thomas, 1976). Changes in brightness (ΔB) are associated with most LU changes, especially constructed related changes. TC results can be physically interpreted as its coefficients are predetermined and independent of each image scene, while PCA coefficients are not. However, for the purpose of simply detecting change/no-change areas, PCA is better than TC in many cases, although the physical interpretation is difficult. TC transformations were performed on Landsat TM (1992) and ETM+ (2000) data.
- ***Image Differencing*** (ID) – ID is effective for identifying LU changes from visible and NIR band pairs acquired in similar circumstances (imaging conditions) using same sensor over two different time periods (Macleod and Congalton, 1998). IRS LISS-III (1999 and 2006) data were used to visualise the LU changes through ID.

*2.3.3 Derivation of LST from Landsat TM and Landsat ETM+*

LST were computed (Weng et al., 2004) from TIR bands (Landsat TM and ETM+). Emissivity correction for the specified LC is carried out using surface emissivities as per Synder et al., (1998); Stathopoplou et al., (2007) and Landsat 7 science data user's handbook (2008). The emmissivity corrected land surface temperature (Ts) are computed as per Artis and Carnahan (1982)

$$T_s = \frac{T_B}{1 + (\lambda \times T_B / \rho) \ln \varepsilon}$$

Equation 1

Where, λ is the wavelength of emitted radiance for which the peak response and the average of the limiting wavelengths (λ = 11.5 μm) (Markham and Barker, 1985) were used, $\rho$ = h x c/σ (1.438 x $10^{-2}$ mK), σ = Stefan Bolzmann's constant (5.67 x $10^{-8}$ $Wm^{-2}K^{-4}$ = 1.38 x $10^{-23}$ J/K), h = Planck's constant (6.626 x $10^{-34}$ Jsec), c = velocity of light (2.998 x $10^{8}$ m/sec), and ε is spectral emissivity.

*2.3.4 LST from MODIS*

MODIS LST/Emissivity 16-bit unsigned integer data with 1 km spatial resolution are multiplied by a scale factor of 0.02 (http://lpdaac.usgs.gov/modis-/dataproducts.asp#mod11) and are converted to degree Celsius.

*2.3.5 NDVI from Landsat TM, ETM+ and MODIS*

NDVI was computed using visible Red (0.63 – 0.69 µm) and NIR (0.76 – 0.90 µm) bands of Landsat TM (1992)/ETM+ (2000) and Red (0.62 – 0.68 microns) and NIR (0.77 – 0.86 microns) bands of LISS-III data of 2006.

*2.3.6 Estimation of abundance maps*

Linear unmixing method was adopted for solving the mixed pixel problem as the spectral radiance measured by a sensor consists of the mixture of radiances reflected in proportion to the sub-pixel area covered (Kumar et al., 2008). Endmembers corresponding to pure pixels are given by the reference spectra of each of the individual pure materials. Spectra corresponding to sub-pixel areas in a pixel are assumed to be linearly independent, and the target pixel spectra are a combination of these spectra (which is proportional to respective LC in a pixel). The spectrum measured by a sensor is a linear combination of the spectra, therefore,

$$y_i = \sum_{j=1}^{n} (a_{ij} x_j) + e_i$$

Equation 2

where $n$ = the number of distinct LU classes; $y_i$ = Spectral reflectance of respective pixels in a band; $a_{ij}$ = Spectral reflectance of the $j^{th}$ component in the pixel for $i^{th}$ spectral band; $x_j$ = Proportion value of the $j^{th}$ component in the pixel; j = 1, 2, 3 ... n (number of land classes assumed); $i$ = 1, 2, 3 ... m (number of multispectral bands) and $e_i$ = error term for the $i^{th}$ spectral band. The error term ($e_i$) is due to the assumption made that the response of each pixel in any spectral wavelength is a linear combination of the proportional responses of each component. Assuming that the error term is 0, equation 2 can be written as:

$$AX=Y$$

Equation 3

where A is a $m$ x $n$ matrix ($a_{11}$, $a_{12}$, …, $a_{mn}$), X is a $n$ x 1 vector ($x_1$, $x_2$, …, $x_n$) and Y is a $n$ x 1 vector ($y_1$, $y_2$, …, $y_n$) written as:

$$\begin{bmatrix} a_{11} & a_{12} & \dots & a_{1n} \\ a_{21} & a_{22} & \dots & a_{2n} \\ \vdots & \vdots & \vdots & \vdots \\ a_{m1} & a_{m2} & \dots & a_{mn} \end{bmatrix} \begin{bmatrix} x_1 \\ x_2 \\ \vdots \\ x_n \end{bmatrix} = \begin{bmatrix} y_1 \\ y_2 \\ \vdots \\ y_n \end{bmatrix}$$

Equation 4

$$X_{constrained} = (A^T A)^{-1} A^T Y + \frac{(1 - 1^T((A^T A)^{-1} A^T Y))}{1^T (A^T A)^{-1}} (A^T A)^{-1} 1$$

Equation 5

Equation 5 gives the Constrained Least Squares (CLS) estimate of the abundance expressed in terms of matrix A, X and Y. The reflected spectrum of a pure feature is called a reference or endmember spectrum. Endmembers are extracted using scatter plot or through automatic endmember extraction techniques (Kumar et al., 2008).

*2.3.7 LC derivation from abundance values along with training polygons using Bayesian classification*

Abundances of each category (pixel wise) are used as a prior probability of the class. In the Baye's classifier for the multispectral data, the posterior probability of the class given the observation is computed by multiplying the prior probability of the class with the conditional probability P(x|k), where $x$ denotes the multispectral observation vector and $k$ any class. The class label assigned to the pixel is:

$$l = \arg \min_k \frac{P(k \mid i, j) P(x \mid k)}{P(x)}$$

Equation 6

**3. Results**

Temporal LU details are displayed in figure 2 and class statistics are listed in table 1. The classified images of 1973, 1992, 1999, 2000, 2002, 2006 and 2007 showed an overall accuracy of 72%, 75%, 71%, 77%, 60%, 73% and 55%. Accuracy assessment was performed which showed higher accuracy for high resolution data (~ 70-75% for Landsat and IRS LISS-III) and decreasing accuracy with coarse spatial resolution (~ 55-60% for MODIS). Figure 3 (a) – (f) depicts the LU change based on differencing techniques of PCA and TC. The disappearance of water bodies from 1973 to 2006 is given in Figure 4. 55% decline (from 207 to 93) in the number of water bodies and 61% decline in the spatial extent (of water bodies) is noticed from the temporal analysis. Validation was done considering training data and Google Earth image, covering approximately 15% of the study area. Then, pixels corresponding to urban category were extracted for further analysis. Figure 5 shows the LST and NDVI of Greater Bangalore in 1992, 2000 and 2007. The minimum (min) and maximum (max) temperature was 12 °C and 21 °C with a mean of 16.5±2.5 from Landsat TM (1992, winter). Similarly MODIS data of 2000 (summer) show the min, max and mean temperature of 20.23, 28.29 and 23.71±1.26 °C respectively. Corresponding values for 2007 (summer) are 23.79, 34.29 with a mean of 28.86±1.60 °C. LC wise NDVI and LST are listed in table 2.

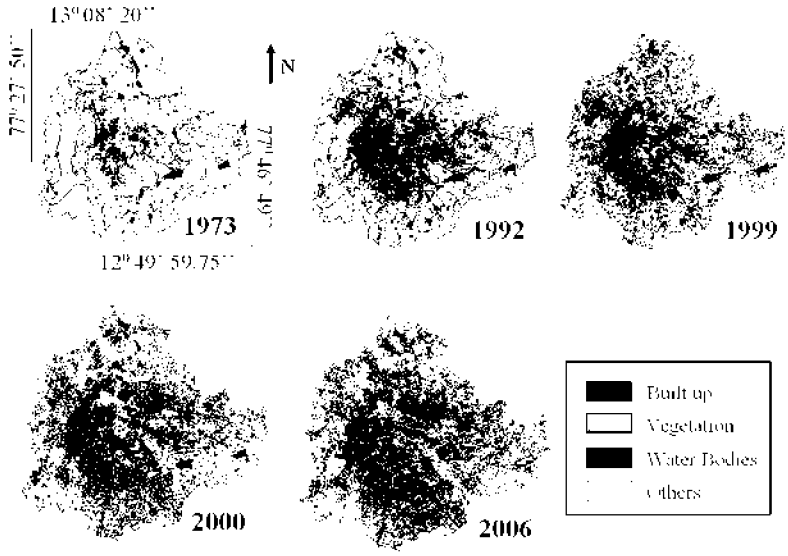


Figure 2: Greater Bangalore in 1973, 1992, 1999, 2000 and 2006

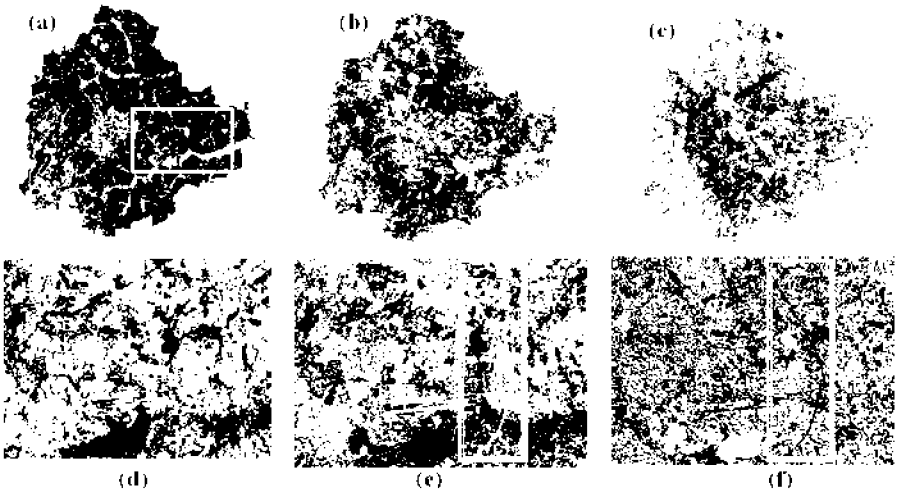


Figure 3: PC1 of Landsat MSS-1973 (a), PC1 of IRS LISS-III-2006 (b) and the change in LU is highlighted in (c) using PCA differencing method. The highlighted box in (a) and (b) are further enlarged in (d) to (f). Brightness values from TC transformation on Landsat TM-1992 (d) and ETM+2000 (e). The changes are highlighted in (f) by differencing the brightness values emphasizing new built up

Table 1: Greater Bangalore land cover statistics

| Class → Year ↓ | | Built up | Vegetation | Water Bodies | Others |
|---|---|---|---|---|---|
| 1973 | Ha | 5448 | 46639 | 2324 | 13903 |
| | % | 7.97 | 68.27 | 3.40 | 20.35 |
| 1992 | Ha | 18650 | 31579 | 1790 | 16303 |
| | % | 27.30 | 46.22 | 2.60 | 23.86 |
| 1999 | Ha | 23532 | 31421 | 1574 | 11794 |
| | % | 34.44 | 45.99 | 2.30 | 17.26 |
| 2000 | Ha | 24163 | 31272 | 1542 | 11346 |
| | % | 35.37 | 45.77 | 2.26 | 16.61 |
| 2002 | Ha | 26992 | 28959 | 1218 | 11153 |
| | % | 39.51 | 42.39 | 1.80 | 16.32 |
| 2006 | Ha | 29535 | 19696 | 1073 | 18017 |
| | % | 43.23 | 28.83 | 1.57 | 26.37 |
| 2007 | Ha | 30876 | 17298 | 1005 | 19143 |
| | % | 45.19 | 25.32 | 1.47 | 28.01 |

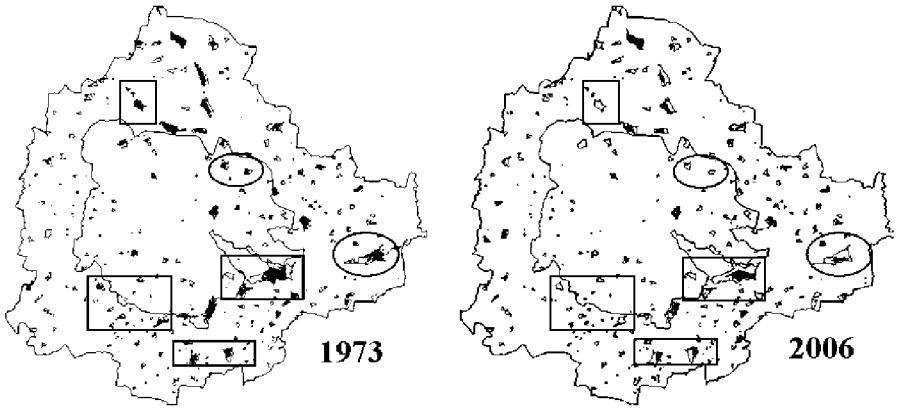


Figure 4: Temporal changes in water bodies from 1973 (using Landsat MSS) to 2006 (using IRS LISS-III) highlighted in rectangular boxes and circles.

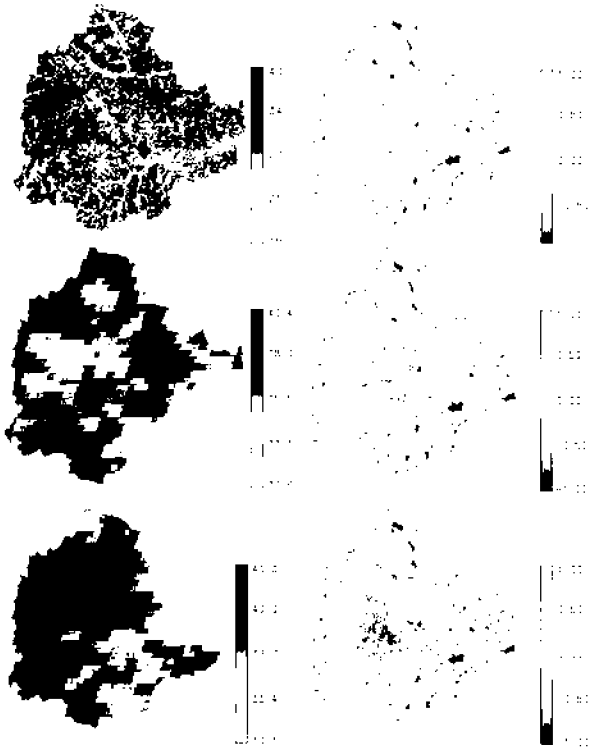

Figure 5: LST from Landsat TM (1992), MODIS (2000 and 2007), NDVI from Landsat TM (1992), Landsat ETM+ (2000) and IRS LISS-III (2006)

Table 2: NDVI and LST (°C) for respective land uses

| Land cover | 1992 (TM) | | 2000 (MODIS) | | 2007 (MODIS) | |
|---|---|---|---|---|---|---|
| | Mean LST (SD) | Mean NDVI (SD) | Mean LST (SD) | Mean NDVI (SD) | Mean LST (SD) | Mean NDVI (SD) |
| **Builtup** | 19.03 (1.47) | -0.162 (0.096) | 26.57 (1.25) | -0.614 (0.359) | 31.24 (2.21) | -0.607 (0.261) |
| **Vegetation** | 15.51 (1.05) | 0.467 (0.201) | 22.21 (1.49) | 0.626 (0.27) | 25.29 (0.44) | 0.348 (0.42) |
| **Water bodies** | 12.82 (0.62) | -0.954 (0.055) | 21.27 (1.03) | -0.881 (0.045) | 24.00 (0.27) | -0. 81 (0.27) |
| **Open ground** | 17.66 (2.46) | -0.106 (0.281) | 24.73 (1.56) | -0.016 (0.283) | 28.85 (1.54) | -0.097 (0.18) |

The relationship between LST and NDVI were investigated for each LC type through the Pearson's correlation coefficient (CC) at a pixel level, which are listed in table 3. It is apparent that values tend to negatively correlate with NDVI for all LC types. NDVI values ranges from -0.05 to -0.6 (built up) and 0.15 to 0.6 (vegetation). Temporal increase in temperature with the increase in the number of urban pixels is noticed during 1992 to 2007 (63%) and 'r' confirms this relationship for the respective years. The decrease in vegetation is reflected by the respective increase in temperature. Further analysis is done by considering vegetation abundance. Landsat ETM+ (band 1, 2, 3, 4, 5 and 7) were unmixed to get the abundance maps of 5 classes (1) dense urban (commercial/industrial/residential), (2) mixed urban (urban with vegetation and open ground), (3) vegetation, (4) open ground and (5) water bodies. We considered only dense urban, mixed urban and vegetation abundance for further analysis as shown in figure 6. The min and max temperature from ETM+ data was 13.49 and 26.32 °C with a mean of 21.75±2.3. These abundance images were further analysed to see their contribution to the UHI by separating the pixels that contains 0-20%, 20-40%, 40-60%, 60-80% and 80-100% of the commercial/industrial/residential (dense urban), mixed urban and vegetation. Table 4 gives the mean and standard deviation (SD) of the LST for various LU. Application of decision based unmixing approach, systematically exploited the information from both the sources (sub-pixel class proportions and classified image based on training data collected from the ground) for achieving more reliable classification, shown in figure 7. Table 5 lists LC wise LST, NDVI and correlation coefficient. Relationship of population density with LST (Landsat ETM+) is evident in figure 8, which corroborate that the increase in LST is due to urbanisation and consequent increase in population.

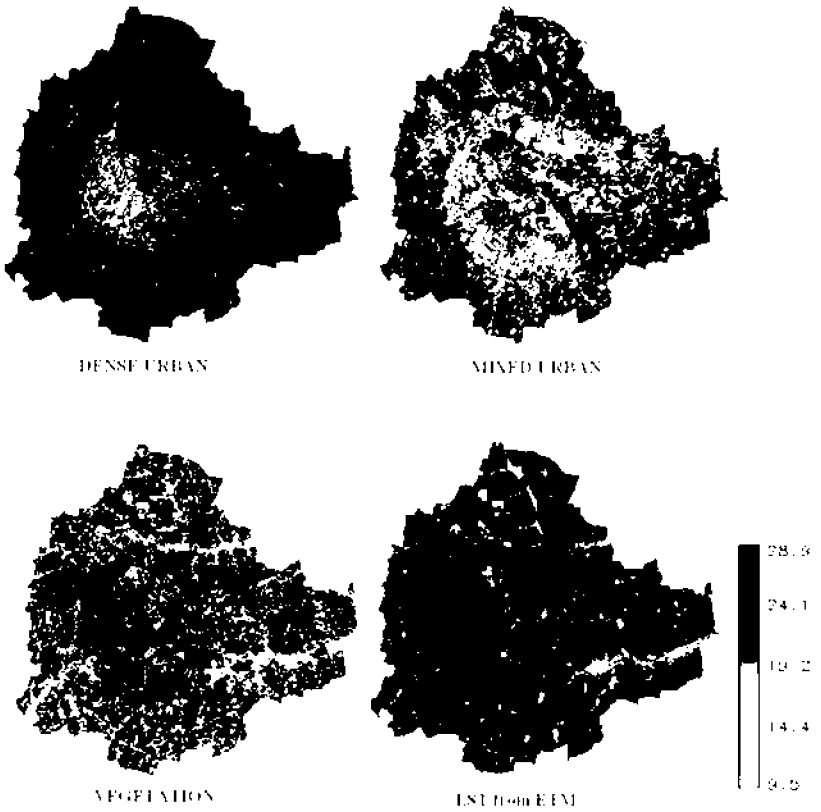


Figure 6: Abundance maps and LST obtained from Landsat ETM+ data (2000)

Table 3: Correlation coefficients between LST and NDVI by LC type (significant at 0.05 level)

| LU | 1992 | 2000 | 2007 |
|---|---|---|---|
| Builtup | -0.7188 | -0.7745 | -0.7900 |
| Vegetation | -0.8720 | -0.6211 | -0.6071 |
| Open ground | -0.6817 | -0.5837 | -0.6004 |
| Water bodies | -0.4152 | -0.4182 | -0.4999 |

Table 4: Mean LST for different LC classes for various abundances

| Class → Abundance ↓ | Mean Temperature ± SD of dense urban | Mean Temperature± SD of mixed urban | Mean Temperature± SD of vegetation |
|---|---|---|---|
| 0-20% | 21.99±2.37 | 21.57±2.36 | 17.91±2.19 |
| 20-40% | 22.06±2.15 | 21.58±2.36 | 17.39±1.37 |
| 40-60% | 22.27±2.00 | 21.67±2.41 | 17.22±0.89 |
| 60-80% | 22.33±2.22 | 22.28±2.02 | 17.13±0.85 |
| 80-100% | 22.47±1.96 | 22.37±2.17 | 17.12±0.91 |

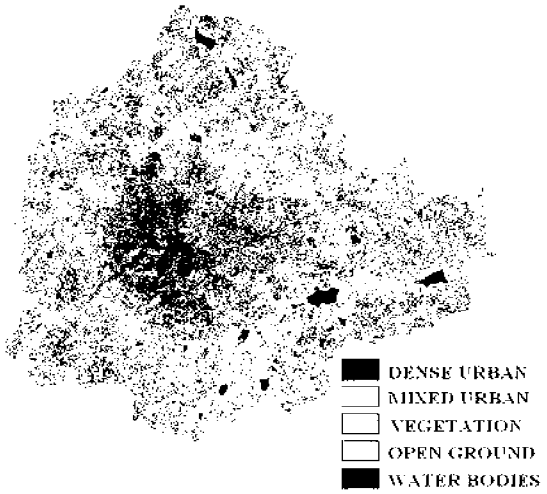


Figure 7: Classified image obtained from combining unmixed images and classified image using spectral signatures from ground as input to Baye's classifier from 6 MSS bands of Landsat ETM+

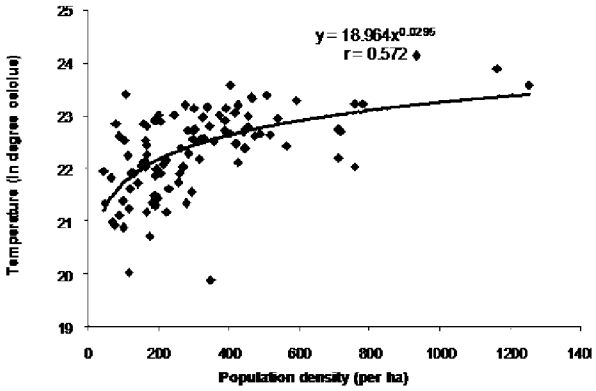


Figure 8: LST with ward wise population density

Table 5: LST, NDVI and correlation coefficient for different LC classes

| Landuse | LST Mean ± SD | NDVI Mean ±SD | Correlation coefficient between LST and NDVI |
|---|---|---|---|
| Dense builtup | 23.09± 1.16 | -0.2904± 0.395 | -0.7771 |
| Mixed builtup | 22.14± 1.06 | -0.138± 0.539 | -0.6834 |
| Vegetation | 19.27± 1.59 | 0.3969± 0.404 | -0.8500 |
| Open Ground | 22.40± 1.97 | -0.0193± 0.164 | -0.6319 |
| Water Bodies | 19.57± 1.72 | -0.301± 0.47 | 0.2319 |

Table 6: MMU sizes for different RS data sources used

| Data source | MODIS | Landsat MSS | Landsat TM/ETM+ | IRS LISS-III |
|---|---|---|---|---|
| MMU (ha) | 6.25 | 0.62 | 0.09 | 0.055 |

## 4. Discussion

The analysis showed that there has been a 466% increase in built up area from 1973 to 2007 as evident from temporal analysis leading to a sharp decline of 61% area in water bodies. LU changes were more prominent in the city during the last 2 decades consequent to rapid urbanisation accompanied with urban sprawl with IT (Information Technology) and BT (Biotechnology) boom and consequent migration of people from different regions. Identification of the changed patches or specific region that underwent changes (from one LU to other) is not easily achievable in a highly dynamic and large urbanising environment considering the varying range of spatial resolutions (23.5 to 250 m) across time (1973 to 2007). This requires the development and maintenance of database for each LU across a large time-scale (Zhang and Zhang, 2007).

A newly constructed flyover or road (for example see a new road in Figure 3 (e) running from south to north highlighted in a rectangular box in the second half of the image), was detected as a broken line in figure 3 (f) due to shadow or getting merged with other classes (mixed pixels), etc. This was obtained by differencing TC transformed 92 and 2000 brightness values and the changed patches were identified using Region Growing Method (RGM) along with thresholding. The exact delineation of the boundary for every recognised change patch also depends on the minimum mapping unit (MMU) and its proper selection (Zhang and Zhang, 2007). Large MMU changes result in significant differences in the accuracy estimates of LC classification. They make change detection more accurate but often miss real and small LU changes. A small MMU present detailed LU changes but also increase the uncertainty of the RS derived change product. MMU for various pixel sizes are listed in table 6. The minimum built up size in residential areas is ~ 0.011 ha to 0.037 ha and often extend up to 1 ha (in case of multi-storied buildings) while industrial buildings can spread from 50 to 150 ha approximately. One way to delineate such features is to perform interactive on-screen editing along with visual interpretation in a synergistic way. MODIS and Landsat MSS present significant challenge due to mixed pixel problems. Landsat TM/ETM+ and IRS LISS-III are adequate for detecting pixel patch changes, yet most of the objects fall on boundaries of two adjacent pixels and they are smaller than the MMU size (form mixed pixels). Hence, these data tend to overestimate the LU classes. The area derived from RS data is closer to the area on the ground when patch size increases. However, area measurements from high spatial resolution were more accurate. The correlation (r) between NDVI and temperature of 1992 (based on TM data) was 0.88. Similarly for 2000, r was 0.72 (MODIS 2000) and 0.65 (MODIS 2007) respectively. Analysis of LST with NDVI suggests that the extent of LC with vegetation plays a significant role in the regional LST. Although many factors can contribute to the variations of LST, the spatial arrangement and aerial extent of various LU types is a fundamental one. Within the city, if we consider the LU nature, then we see that temperature falls from densely builtup area to medium builtup area and again from medium builtup to vegetative land. The temperature close to vegetation and wetlands were lower by 4 and 5-7 °C respectively (see table 2). This highlights that LU characteristics play a significant role in maintaining the ambient temperature and also in the regional heat island phenomenon. Vegetation and water bodies are negatively correlated with temperature suggesting that these LU aid as heat sinks and hence maintains salubrious regional climate. Accuracy of the unmixing decision based approach considering information from sub-pixel class proportions and classified map obtained using training data was 85.46%. This approach is apt for fusing the information obtained from multi-sensors (such as MODIS and IRS). MODIS based sub-pixel information obtained from one of the unmixing techniques can be fused with IRS LISS-III MSS classified information. The endmembers for MODIS data unmixing can be extracted from the image itself (Kumar et al., 2008), while IRS LISS-III MSS classification is done with the training data. This technique would be helpful in optimising the benefits of higher spectral and spatial resolutions of multi-sensors. Certain areas in the city with sparsely located building having parks and lakes in the surroundings have lower air temperature compared to completely urbanised regions. UHI is evident with the enhanced surface temperatures in urbanised landscapes compared to their surroundings (non-urbanised). Temperature profile with respect to human population density is depicted in figure 8, suggesting that dense urban areas have higher temperatures. When the population of a region exceeds its carrying capacity, it exerts pressure on the local natural resources (land, water, etc.). Correlations among LST and NDVI are the result of unique signatures of the biophysical parameters due to interactions between thermal and vegetation dynamics in each LU.

## 5. Conclusion

This study analysed the role of increased urbanisation through spatial change analysis on LST, which is positively correlated with urbanising landscapes and negatively correlated with vegetation and water bodies. Abundance maps with pixels having 80-100% dense builtup and mixed builtup class proportions show increase in urban temperature by an average of 2 °C. LST were comparatively lower in areas having parks, healthy vegetation and lakes that aid as heat sinks. Although the algorithms adopted here seems to work satisfactorily, the classification and change detection methods in use were not very suitable for handling multi-sensor, multi-resolution condition as the classification accuracies obtained from MODIS data were low. These require advanced image fusion and LU classification algorithms or machine learning techniques to be adopted to achieve higher classification accuracies. The unmixing decision based approach adopted in this paper is an attempt to achieve classification results with higher

accuracies per class. This could be automated to obtain LU classes and bring out changes across multi-temporal data routinely. Methods of change detection from multi-resolution images integrating spectral, structural and textural features to generate changed patches and change attribute is also desirable and a challenging area of research.

**References**


Artis, D. A., and Carnahan, W. H., 1982, Survey of Emissivity Variability in Thermography of Urban Areas. *Remote Sensing of Environment*, 12, 13-329.

Balling, R. C., and Brazell, S. W., 1988, High Resolution Surface Temperature Patterns in a Complex Urban Terrain. *Photogrammetric Engineering and Remote Sensing*, 54, 289-293.

Carnahan, W. H., and Larson, R. C., 1990, An analysis of an urban heat sink. *Remote Sensing of Environment*, 33, 65-71.

Dash, P., Gottsche, F. M., Olesen, F. S., and Fischer, H., 2002, Land Surface Temperature and Emissivity Estimation from Passive Sensor Data: Theory and Practice-Current Trends. *International Journal of Remote Sensing*, 23(13), 2563–2594.

Duda, R. O., Hart, P. E., and Stork, D. G., 2000, *Pattern Classification*, A Wiley-Interscience Publication, Second Edition, ISBN 9814-12-602-0.

Forghani, A., Cechet, B., and Nadimpalli, K., 2005, Object-Based Classification of Multi-Sensor Optical Imagery to Generate Terrain Surface Roughness Information for Input to wind Risk Simulation. *Proceedings of the Geosciences and Remote Sensing Symposium,* 2007, IGARSS '07, 23-27 July, 2007, Barcelona, Spain, IEEE International Publication, 3090-3095.

Friedl, M. A., 2002, Forward and Inverse Modeling of Land Surface Energy Balance using Surface Temperature Measurements. *Remote Sensing of Environment*, 79, 344-354.

Fung, T., and LeDrew, E., 1987, Application of Principal Component Analysis for Change Detection. *Photogrammetric Engineering and Remote Sensing*, 53(12), 1649-1658.

Gallo, K. P., and Owen, T. W., 1998, Assessment of Urban Heat Island: A Multi-Sensor Perspective for the Dallas-Ft. Worth, USA Region. *Geocarto International*, 13, 35– 41.

Gallo, K. P., McNab, A. L., Karl, T. R., Brown, J. F., Hood, J. J., and Tarpley, J. D., 1993, The use of NOAA AVHRR Data for Assessment of the Urban Heat Island Effect. *Journal of Applied Meteorology*, 32, 899– 908.

Kato, S., and Yamaguchi, Y., 2005, Analysis of Urban Heat-Island Effect using ASTER and ETM+ Data: Separation of Anthropogenic Heat Discharge and Natural Heat Radiation from Sensible Heat Flux. *Remote Sensing of Environment*, 99, 44–54.

Kauth, R. J., and Thomas, G. S., 1976, The Tasseled Cap-A Graphic Description of The Spectral-Temporal Development of Agricultural Crops as seen by LANDSAT. *Proceedings of the Symposium on Machine Processing of Remotely Sensed Data*, Purdue University of West Lafayette, Indiana, 4B-41-4B – 51.

Kidder, S. Q., and Wu, H. T., 1987, A Multispectral Study of the St. Louis Area Under Snow-Covered Conditions using NOAA-7 AVHRR Data. *Remote Sensing of Environment*, 22, 159–172.

Kumar, U., Kerle, N., and Ramachandra T. V., 2008, Contrained Linear Spectral Unmixing Technique for Regional Land Cover Mapping using MODIS Data. *In: Innovations and Advanced Techniques in Systems, Computing Sciences and Software Engineering,* Edited by Khaled Elleithy. Berlin: Springer, ISBN: 978-1-4020-8734-9, 87 - 95.

Landsat 7 Science Data User's Handbook, Landsat Project Science Office, Goddard Space Flight Center, 2002, URL: http://ltwww.gsfc.nasa.gov-/IAS/handbook/handbook_toc.html (last accessed: 25 March, 2008).

Landsbeg, H. E., 1981, *The Urban Climate*, (New York: Academic Press).

Li, F., Jackson, T. J., Kustas, W., Schmugge, T. J., French, A. N., Cosh, M. L., and Bindlish, R., 2004, Deriving land surface temperature from Landsat 5 and 7 during SMEX02/SMACEX. *Remote Sensing of Environment*, 92, 521 – 534.

Lu, D., Mausel, P., Brondizio, E., and Moran, E., 2004, Change Detection Techniques. *International Journal of Remote Sensing*, 25(12), 2365-2407.

Macleod, R. D., and Congalton, R. G., 1998, A Quantitative Comparison of Change-Detection Algorithms for Monitoring Eelgrass from Remotely Sensed Data. *Photogrammetric Engineering and Remote Sensing*, 64(3), 207-216.

Markham, B. L., and Barker, J. K., 1985, Spectral Characteristics of the LANDSAT Thematic Mapper Sensors. *International Journal of Remote Sensing*, 6, 697-716.

Michener, W. K., and Houhoulis, P. F., 1997, Detection of Vegetation Associated with Extensive Flooding in a Forest Ecosystem.

*Photogrammetric Engineering and Remote Sensing*, 63(12), 1363-1374.

Nikolakopoulos, K. G., Vaiopoulos, D. A., and Skianis, G. A., 2003, Use of Multitemporal Remote Sensing Thermal Data for the Creation of Temperature Profile of Alfios River Basin, *Proceedings of the Geoscience and Remote Sensing Symposium, 2003, IGARSS '03*, 21-25 July 2003. IEEE International Publication, 4:2389-2391, ISBN: 0-7803-7929-2.

Ramachandra, T. V., and Kumar, U., 2008, Wetlands of Greater Bangalore, India: Automatic Delineation through Pattern Classifiers. *Electronic Green Journal*, 26, WebURL: http://egj.lib.uidaho.edu/index.php/egj/article/view/3171

Schmugge, T., Hook, S. J., and Coll, C., 1998, Recovering Surface Temperature and Emissivity from Thermal Infrared Multispectral Data. *Remote Sensing of Environment*, 65, 121– 131.

Snyder, W. C., Wan, Z., Zhang, Y., and Feng, Y. Z., 1998, Classification Based Emissivity for Land Surface Temperature Measurement from Space. *International Journal of Remote Sensing*, 19, 2753– 2774.

Stathopoplou, M., Cartalis, C., and Petrakis, M., 2007, Integrating CORINE Land Cover Data and landsat TM for Surface Emissivity Definitions: An Application for the Urban Areas of Athens, Greece. *International Journal of Remote Sensing*, 28, 3291-3304.

Stathopoulou, M., and Cartalis, C., 2007, Daytime Urban Heat Island from Landsat ETM+ and Corine land Cover Data: An application to Major Cities in Greece. *Solar Energy*, 81, 358-368.

Tanaka, Y., Shibata, S., and Gotoh, K., 2005, Appearance Characteristic Analysis of Heat Island Phenomenon by Using Satellite Remote Sensing and GIS. *Proceedings of the Geosciences and Remote Sensing Symposium, 2005, IGARSS '05*, 25-29 July 2005, IEEE International Publication, 3:1855-1858, ISBN: 0-7803-9050-4.

Weng, Q., Lu, D., and Schubring, J., 2004, Estimation of Land Surface Temperature – Vegetation Abundances Relationship for Urban Heat Island Studies. *Remote Sensing of Environment*, 89, 467-483.

*WUP (World Urbanization Prospects): The 2005 Revision*, Population Division, Department of Economic and Social Affairs, UN.

Zhang, J., and Zhang, Y., 2007, Remote Sensing Research Issues of the National Land Use Change Program of China. *Photogrammetry & Remote Sensing*, 62(6), 461-472.